Compact Co-Linearly Polarized Microstrip Antenna With Fence-Strip Resonator Loading for In-Band Full-Duplex Systems

Yijing He, *Graduate Student Member, IEEE*, and Yue Li, *Senior Member, IEEE*

***Abstract*— A compact co-linearly polarized microstrip antenna with identical radiation properties is proposed and validated for in-band full-duplex systems. By exploring a fence-strip resonator (FSR) in the central plane of a patch, good isolation is achieved between the transmitting and receiving ports. The proposed FSR consists of a metallic vias fence and a strip with a distance away from the ground, performing as a pair of distributed inductor and capacitor. When the FSR is resonating, the radiating current is concentrated in the half part of the patch, performing at its half-TM_{10} mode with high port isolation. To validate the proposed antenna, a prototype with the size of $0.25\lambda_0 \times 0.25\lambda_0 \times 0.04\lambda_0$ (λ_0 is the free-space wavelength at center frequency) has been fabricated and characterized, with experiments consistent well with simulations. A measured port isolation higher than 20 dB is achieved over the operating bandwidth of 2.40–2.52 GHz with the maximum of 30 dB. The proposed antenna is with the merits of compact size, low profile, simple feed, and planar-integrated structure for in-band full-duplex systems.**

***Index Terms*— Antenna radiation patterns, full-duplex antennas, microstrip antennas, mutual coupling, resonator.**

I. Introduction

NOWADAYS, the electromagnetic spectrums in the wireless communication become increasingly congested, and the remaining deployable bands are highly precious. Emerging as the times require, in-band full-duplex or simultaneous transmit and receive (STAR) systems have attracted tremendous attention as a promising method to increase spectrum efficiency [1]–[5]. Compared with frequency-division and time-division duplex systems, the spectral efficiency of in-band full-duplex systems is doubled with transmitter and receiver cooperation. To make full-duplex systems available in practical engineering, high isolation between the transmitter and receiver is required and are usually achieved by the joint support from digital, analog, and antenna domains [6]–[8].

Manuscript received September 7, 2020; revised November 19, 2020; accepted December 20, 2020. Date of publication January 20, 2021; date of current version October 28, 2021. This work was supported in part by the National Natural Science Foundation of China under Grant 61771280; in part by the Youth Top Program of Beijing Outstanding Talent Funding Project; and in part by the National Key Research and Development Program of China under Grant 2018YFB1801603. *(Corresponding author: Yue Li.)*

The authors are with the Department of Electronic Engineering, Tsinghua University, Beijing 100084, China, and also with the Beijing National Research Center for Information Science and Technology, Tsinghua University, Beijing 100084, China (e-mail: lyee@tsinghua.edu.cn).

Color versions of one or more figures in this article are available at https://doi.org/10.1109/TAP.2021.3051380.

Digital Object Identifier 10.1109/TAP.2021.3051380

As the front end of full-duplex systems, antennas with high isolation can relieve the pressure on subsequent analog and digital domains. In past decades, various techniques have been investigated and reported to enhance the isolation between the transmitting (TX) and the receiving (RX) antennas. In general, these designs are classified into several categories: the first one separates TX and RX apertures physically by a large distance, i.e., involving bistatic antennas, which usually adopt spatial diversity [9], [10]. This approach is simple, but limited by the large antenna dimension. Polarization multiplexing [11]–[25] and pattern diversity [26] are also exploited to achieve high isolation at the cost of using different polarizations and radiation patterns, respectively. The third method employs near-field cancellation [27]–[31], which often places one antenna at the near-field null of the other antenna to obtain high isolation with dissimilar radiation patterns. Apart from the mentioned methods above, decoupling network or surface [32]–[40] such as electromagnetic bandgap (EBG) structures [34], [35], high-rejection filters [36], resonators [38]–[40] are added between TX and RX antennas to suppress the electromagnetic coupling. Finally, circulators or butler matrix beamforming networks (BFNs) [41]–[51] are also employed for orthogonal phase modes to achieve monostatic STAR configuration. This approach has rigorous requirements for the return loss and isolation of the circulators and BFNs. These techniques usually adopt antenna arrays or multiple separated antennas, thus occupying large physical size or bulky geometry. Some antennas using orthogonal mode transducer (OMT) [10], [11] obtained high isolation without large size, at the cost of using polarization multiplexing. To date, few works have been reported on in-band full-duplex antennas with a compact size, and without using multiplexing techniques. In [28], a co-vertically polarized STAR antenna was achieved with a compact diameter size of $0.44\lambda_0$, possessing a bulky structure and high profile of $0.15\lambda_0$. In [45], a co-horizontally polarized in-band full-duplex dipole array was presented with a compact size of $0.38\lambda_0 \times 0.38\lambda_0$, but also with a bulky profile of $0.15\lambda_0$. To sum up, to achieve in-band full-duplex antennas with compact size, low profile, and without using multiplexing techniques is still a challenging and long-sought goal.

In this article, a compact co-linearly polarized microstrip antenna with low profile and identical radiation properties for in-band full-duplex systems is proposed, as shown in Fig. 1. By loading a fence-strip resonator (FSR) in the central plane

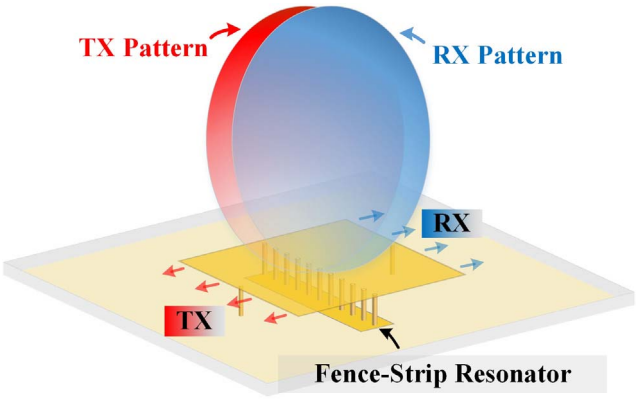

Fig. 1. General concept of the proposed microstrip antenna for in-band full-duplex systems.

of a patch with typical footprint, good isolation is achieved for the TX and RX ports within a very compact size of $0.25\lambda_0 \times 0.25\lambda_0$ and a low profile of $\times 0.04\lambda_0$. Here, the proposed FSR is composed by a metallic vias fence and a strip with a distance away from the ground, serving as a pair of series distributed inductor and capacitor. When the FSR is resonating, the radiating current is concentrated on the half part of the patch, performing at its half-TM_{01} mode with high isolation. For validation, a prototype has been fabricated and characterized, with the measurements agreeing well with simulations. The measured port isolation over 20 dB and the maximum of 30 dB are achieved over the operating bandwidth ($|S_{11}| < -10$ dB) of 2.40–2.52 GHz. The proposed antenna is with the merits of compact size, low profile, and simple feeding, promising usage for in-band full-duplex systems.

The novelty and contributions of this work are summarized as follows. First, good isolation between the TX and RX ports of a patch antenna is achieved within a compact size of $0.25\lambda_0 \times 0.25\lambda_0$ and a low profile of $0.04\lambda_0$ (λ_0 is the free-space wavelength at center frequency). Second, the proposed antenna is with co-linear polarization and nearly identical radiation patterns, avoiding using polarization multiplexing and pattern diversity. Third, this work also has the advantages of simple feed, easy fabrication, and planar structure.

II. Antenna Design

A. Antenna Configuration

As illustrated in Fig. 2(a), the proposed antenna is composed of a rectangular patch, a centrally loaded FSR structure, and a metallic ground. The FSR is formed by a metallic vias fence and a rectangular metallic strip. Constructed by a standard printed circuit board (PCB) process, the proposed antenna consists of two dielectric substrate layers and three metal layers. The top patch and the middle metallic strip are printed on the top and bottom side of the dielectric substrate layer 1, respectively, and they are connected using the vias fence. All the dielectric substrates used in the proposed antenna are F4BM, with $\varepsilon_r = 2.65 \pm 0.05$ and $\tan\delta = 0.002$. The two dielectric substrate layers have the same dimension of $L_g \times W_g$ (150 mm × 150 mm) as the metallic ground. For the fabricated prototype, these two layers are fixed together using Nylon screws.

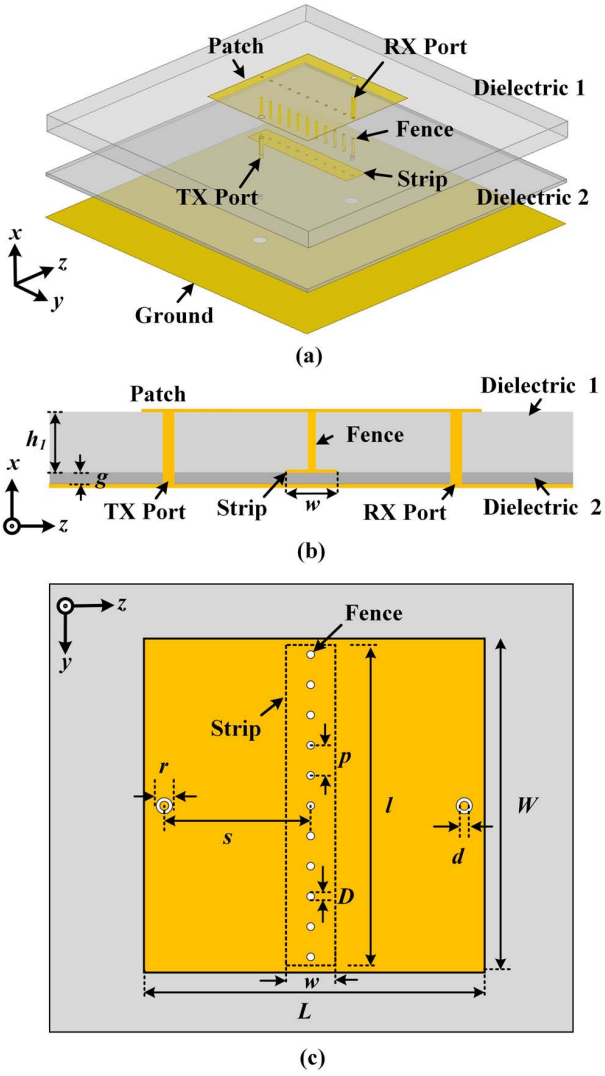

Fig. 2. (a) Exploded view. (b) Cross-section view. (c) Top view of the proposed antenna.

Fig. 2(b) and (c) presents the cross-section and top view of the proposed antenna, respectively. The proposed FSR is exploited to load in the central plane of the microstrip antenna. The fence consists of a row of metallic through vias with identical diameter D, and these vias are homogenously distributed with period p along the central line. For the proposed antenna, eleven through vias are employed for this fence. Printed on the bottom side of the dielectric substrate layer 1, the metallic strip is denoted by the dashed-line rectangular box in Fig. 2(c). Besides, two metallic feeding probes are symmetrically employed for the proposed antenna to excite the TX and RX ports, respectively. Here, a ring gap is also adopted for the impedance matching of the two feeding ports. All the geometric parameters of the proposed antenna shown in Fig. 2 are listed in Table I.

B. Operating Principle

The evolution process is explained in detail to bright more insight into the operating principle of the proposed antenna. As illustrated by the concept in Fig. 1, the proposed antenna

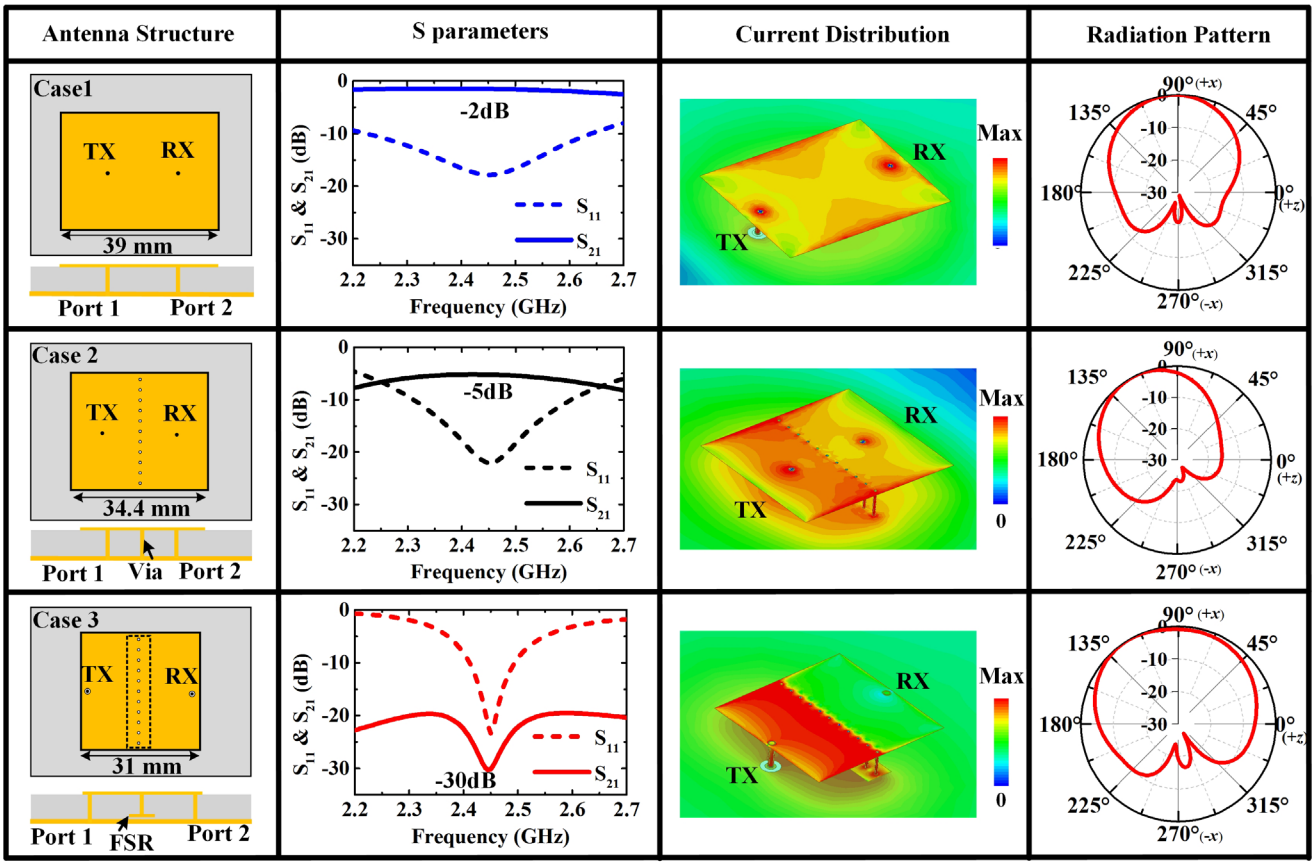

Fig. 3. Comparison of a regular microstrip antenna, a vias-loaded microstrip antenna, the proposed antenna, and their corresponding simulated *S* parameters and complex surface current distributions.

TABLE I

DIMENSIONS OF THE PROPOSED ANTENNA IN FIG. 1 (UNIT: mm)

p	D	s	d	W	L	r	w	l	g	h_1
2.8	0.6	14.2	1.2	30.5	31	1.6	5.8	30.2	0.254	5.0

achieves identical radiation properties for the TX and RX ports, with co-linear polarization and compact size for in-band full-duplex systems. To demonstrate the evolution process and good performances of the proposed antenna, Fig. 3 presents the comparison of the antenna structure, *S* parameters, complex surface current distribution, and radiation pattern among three different cases. These three cases are: 1) the regular microstrip antenna with the TX and RX ports; 2) the regular microstrip antenna with a centrally loaded through-via fence, and the TX and RX ports; and 3) the proposed antenna with the centrally loaded FSR, and the TX and RX ports. For fair and convincing comparison, these antennas are with identical profile of $0.04\lambda_0$, and operate at the same center frequency of 2.46 GHz. Besides, these three cases are configured with the same metallic ground with the size of 150 mm × 150 mm (approximately $1.23\lambda_0 \times 1.23\lambda_0$). The TX and RX ports of these antennas are fed by two symmetrical feeding probes. Good impedance matching is obtained for these three cases. Last but not least, here, it is assumed that only TX port is excited for these three cases.

First, case 1 shows the regular microstrip antenna with the TX and RX ports, and its simulated performances. From the *S* parameters, it can be seen that this antenna has strong coupling between the TX and RX ports, only with an isolation of approximately 2 dB. This poor performance is also validated by the almost same surface current magnitude distributions on the left and right half of the patch. At this time, the antenna has a broadside radiation pattern same as the traditional TM_{10}-mode microstrip antenna, indicating that both radiation apertures of the patch are functioning. Based on case 1, case 2 studies a regular microstrip antenna loaded with a vias fence in the central plane. The vias fence consists of a row of metallic through vias with identical diameter D and period p. It is seen that the port isolation is improved slightly to 5 dB. Unfortunately, a strong current still exists on the right half of the patch, indicating tremendous coupling for the two ports. What is worse, it is seen that the E-plane beam has an obvious squint angle owing to the strong coupling between TX and RX ports. The beam squint happens because both radiating apertures are excited by the strong coupling between TX and RX antennas. Meanwhile, there exists phase difference between the two radiating apertures, thus leading to obvious beam squint.

Case 3 presents the proposed compact co-linearly polarized microstrip antenna with identical radiation properties for in-band full-duplex systems. Here, a FSR is loaded in the central plane of a regular patch. The proposed FSR contains a metallic

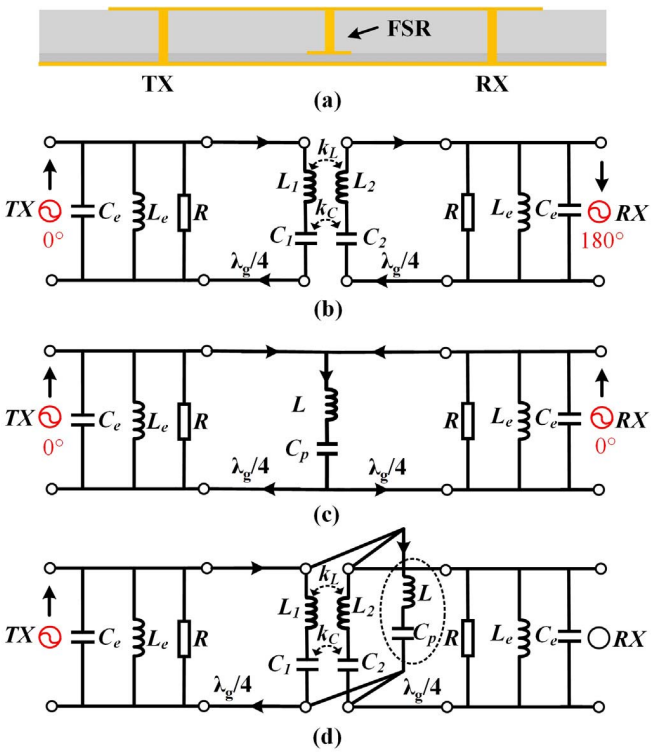

Fig. 4. (a) Proposed antenna. (b) Differential-mode. (c) Common-mode. (d) Overall equivalent circuit models of the proposed antenna.

vias fence and a metallic strip. The fence here also consists of a row of identical metallic vias, homogenously loaded along the central plane. The metallic strip is with a distance away from the ground, and connected with the top patch by the vias fence. Interestingly, it is seen that the isolation between the TX and RX ports is significantly enhanced to 30 dB at the center frequency of 2.46 GHz. It is also observed that there exists a huge contrast between the current distributions on the left and right half part of the patch. In addition, compared with cases 1 and 2, the proposed antenna demonstrates a better broadside radiation property with wider beamwidth, due to that only one radiating aperture functions. For the proposed antenna, the radiation pattern has only a small squint angle and becomes more symmetrical about the broadside angle, contributed to the good decoupling between the TX and RX antennas. At this time, only the TX aperture is radiating, actually behaving as a single planar inverted-F antenna (PIFA).

To explain the operating mechanism of the proposed antenna more clearly, the differential-mode, common-mode equivalent circuits, and overall equivalent circuit are illustrated in Fig. 4. According to the classical model of the microstrip antenna [52], the radiating apertures can be modeled as parallel *RLC* circuits. As seen, C_e denotes the equivalent capacitance of the fringe field, L_e presents the equivalent inductor, and R is the radiating resistor. The symmetrical antenna structure also leads to the symmetric equivalent circuit model. Fig. 4(b) illustrates the differential-mode equivalent circuit of the proposed antenna when TX and RX ports are fed with same-amplitude and anti-phase excitation. At this time, the coupling between the TX and RX patch can be modeled as coupling inductors L_1 and L_2, and coupling capacitors C_1 and C_2. Two parameters k_L and k_C represent the coupling coefficients of the inductors L_1 and L_2, and capacitors C_1 and C_2, respectively. Fig. 4(c) presents the common-mode equivalent circuit when the TX and RX ports are fed with same-amplitude and in-phase excitation. At this time, the FSR performs as a pair of series distributed inductor and capacitor, resonating at the same frequency with the TX and RX patch. A zero-impedance current path is established in the middle of the circuit. Therefore, it can be concluded that there is no coupling between TX and RX ports when the patch operates at common-mode state. Fig. 4(d) demonstrates the overall equivalent circuit of the proposed antenna when only TX port is excited. The equivalent circuit can be viewed as the superposition of the differential-mode and common-mode equivalent circuits. A zero-impedance current path is formed in the central plane of the equivalent circuit when the FSR resonates with the TX patch. As a result, the radiating current is concentrated on the left half part of the patch, performing at its half-TM_{10} mode with high isolation. At this time, the inductive and capacitive coupling between the TX and RX patches are effectively suppressed. This is the fundamental decoupling mechanism of the proposed compact antenna for in-band full-duplex systems.

C. Design Guideline

Here, the design guideline of the proposed antenna is summarized. First, set the initial dimensions of a regular microstrip antenna approximately as $0.5\lambda_g \times 0.5\lambda_g$ at f_0 (λ_g is the guided wavelength in the dielectric, f_0 is the target frequency). Second, load the FSR in the central plane of the patch. The number, diameter, period of the vias fence, strip size, and its gap to ground should be properly selected to offer suitable inductor and capacitor for the series *LC* resonator. The vias fence and strip can be cooperatively designed to make the FSR resonate at same frequency with the half-TM_{10}-mode patch (pretty much similar to a PIFA). Finally, refine the dimensions of the FSR to locate the operating frequency of the half-TM_{10}-mode patch and the FSR at the same frequency f_0.

III. Numerical Study and Discussion

In this section, some important structural parameters are studied to find their influences on the performances of the proposed antenna. Fig. 5 reports the simulated impedance properties of the proposed antenna from 2.2 to 2.7 GHz with different feeding schemes and locations. It is noted that all these impedance property curves in the Smith chart of Fig. 5 have been normalized to 50 Ω. As depicted in Fig. 5(a), when the antenna is fed directly by a probe, i.e., without the ring gap shown in the inset, the impedance curve is totally not matched. However, by observing the location of the impedance curve, it is possible to move the impedance point of 2.46 GHz roughly to the center matching point of Smith chart through adding a series capacitor. This expectation is then validated by adding a small ring gap with an outer diameter $r = 1.6$ mm to the feeding probe. The impedance curve after matching is shown by the red line. Fig. 5(b) presents the simulated impedance properties of the proposed antenna with different feeding

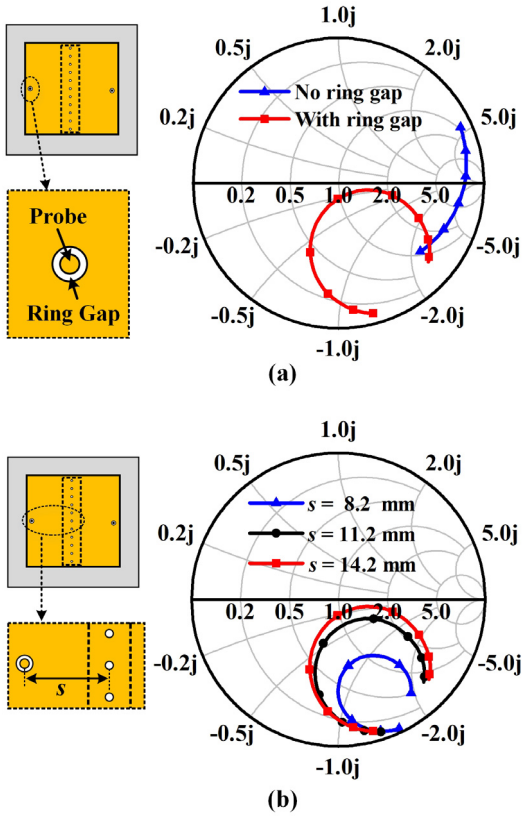

Fig. 5. Impedance property of the proposed antenna (a) with or without the ring gap and (b) under different feeding location s.

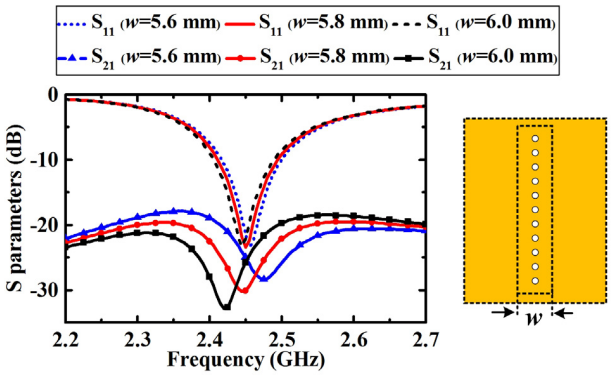

Fig. 6. Simulated S parameters of the proposed antenna with different width w for the strip.

location s. It is seen that when $s = 14.2$ mm, the impedance property of the proposed antenna can be matched at 2.46 GHz.

Fig. 6 and 7 study the effects of geometric parameters of the metallic strip on the S parameters of the proposed antenna. As seen in Fig. 6, when the width w of the strip varies from 5.6 to 6.0 mm, the dip of the isolation curves (i.e., S_{21}) gradually moves to a lower frequency. This phenomenon is because increasing width w of the metallic strip enlarges the capacitance value of the equivalent capacitor, thus the center resonance frequency of the FSR can be reduced. These results also imply that the frequency of the FSR can be tuned independent of the half-TM_{10}-mode patch. Fig. 7 discusses the influence of the gap g between the strip and ground on

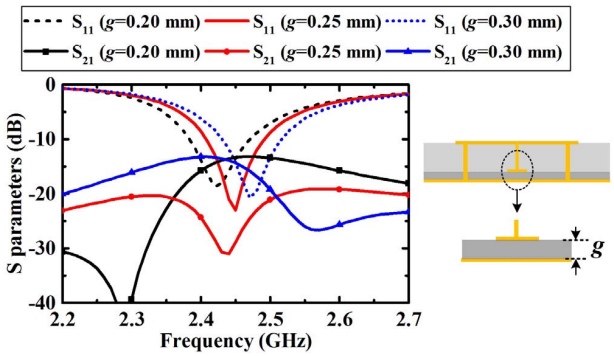

Fig. 7. Simulated S parameters of the proposed antenna with different gap g for the strip.

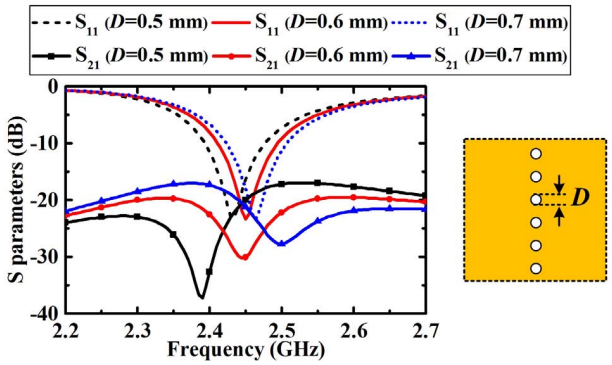

Fig. 8. Simulated S parameters of the proposed antenna with different diameter D for the vias fence.

the S parameters of the proposed antenna. It can be concluded that the gap g is an important parameter to tune the equivalent capacitance of the strip capacitor. Meanwhile, it is also found that only when the center resonance frequency of the FSR agrees with that of the half-TM_{10}-mode patch, good isolation between the TX and RX ports can be achieved.

Fig. 8 and 9 investigate the influences of the structural parameters of the vias fence on the S parameters. It is seen that smaller diameter D leads to the lower dip frequency of the isolation curves. This trend is owing to that the smaller diameter D of the vias results in a larger equivalent inductor of the vias fence, therefore, a lower center resonance frequency of the FSR. Fig. 9 reports the effect of the period p of the vias fence on the S parameters of the proposed antenna. It is noted here that the number of the metallic vias is fixed to eleven. The antenna can achieve good port isolation of approximately 30 dB when $p = 2.8$ mm, where the resonance frequency of the FSR coincides with that of the half-TM_{10}-mode patch. Hence, for better isolation performance, it is necessary for the resonance frequency of the loaded FSR to keep consistent with that of the half-TM_{10}-mode patch.

IV. Experimental Results

To validate the proposed antenna, a prototype is fabricated and experimentally characterized. Fig. 10 illustrates the photographs of the fabricated and assembled prototype. Fig. 10(a) and (b) presents the top and bottom view of the fabricated dielectric substrate layer 1, respectively, while

TABLE II
COMPARISONS BETWEEN THE PROPOSED ANTENNA AND OTHER REPORTED WORKS

Reference	Antenna type	Polarization	Method	Dimension (λ_0^3)	Bandwidth (%)	Isolation (dB)	Planar Integration?	Feeding Scheme
[27]	Monocone+loops array	Co-linearly	Near-field cancellation	1.51×1.54×0.47	98%	>40	No	Quadrifilar IC
[28]	Monopole+loops	Co-linearly	Near-field cancellation	π $(0.44)^2$×0.15	11.7%	>38	No	Quadrifilar IC
[29]	2×2 patch array	Co-circularly	Near-field cancellation	2.42×2.42×0.08	18.2%	>40	Yes	Feeding network
[31]	2×2 patch array	Co-circularly	Phase orthogonality	1.0×1.0×0.03	4.0%	>40.6	Yes	Feeding network
[44]	Circular dipole array	Co-circularly	Phase orthogonality	1.29×0.40×0.27	5.5%	>24	No	BFN
[47]	2×2 patch array	Co-circularly	Phase orthogonality	2.05×2.05×0.04	6.4%	>38	No	Feeding network
This work	Single patch	Co-linearly	Decoupling resonator	0.25×0.25×0.04	4.9%	>20	Yes	Direct feed

Note: λ_0^3 is the free-space wavelength at center frequency.

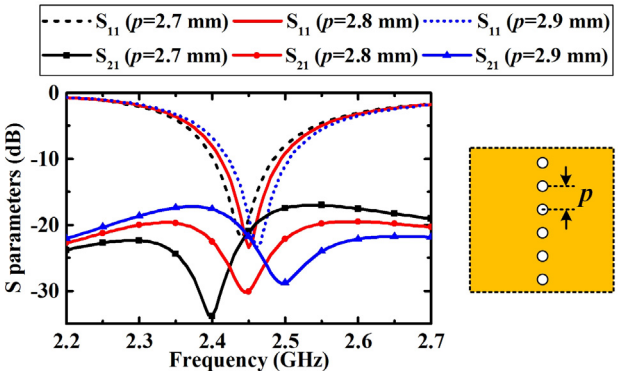

Fig. 9. Simulated S parameters of the proposed antenna with different diameter p for the vias fence.

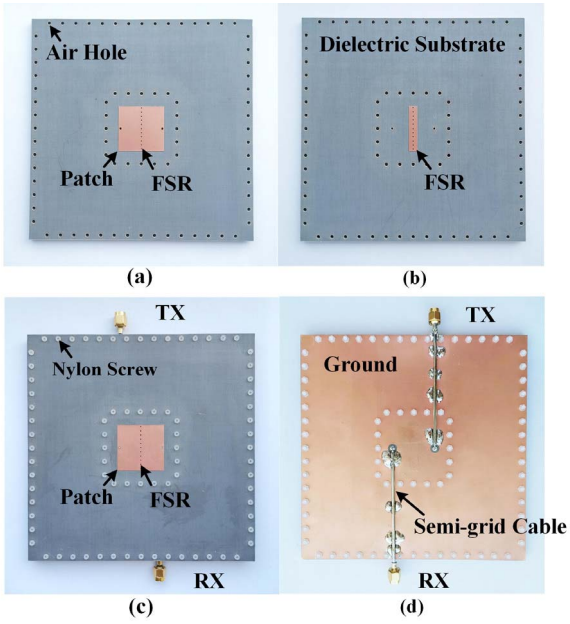

Fig. 10. Photographs of the fabricated antenna prototype. (a), (c) Top and (b), (d) bottom view of the fabricated upper substrate and antenna prototype, respectively.

Fig. 10(c) and (d) shows the top and bottom view of the whole assembled prototype, respectively. The two dielectric substrate layers were fixed together using Nylon screws. Dielectric

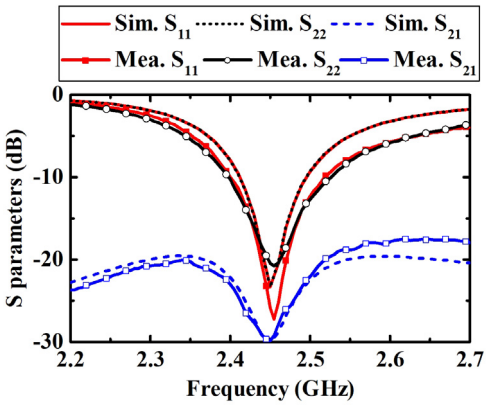

Fig. 11. Simulated and measured S parameters of the proposed antenna.

substrate F4BM ($\varepsilon_r = 2.65 \pm 0.05$, and $\tan\delta = 0.002$) was employed. Two semigrid coaxial cables were used, with the inner conductors soldered on the feeding probes and outer conductors connected with the ground. All detailed geometrical parameters of the fabricated prototype are listed in Table I. The S parameters of the antenna prototype were measured by a vector network analyzer (Agilent N9917A), and the radiation patterns were experimentally tested in the anechoic chamber. Fig. 11 reports the simulated and measured S parameters of the proposed antenna, with two agreeing well with each other. The simulated operating bandwidth ($|S_{11}| < -10$ dB) for the TX and RX ports is 2.41–2.49 GHz, while the measured one for the TX and RX ports covers from 2.40 to 2.52 GHz. The minor differences may be due to the increased loss from the dielectric substrates. Finally, the measured port isolation more than 20 dB and a dip of 30 dB are achieved across the whole operating bandwidth, presenting good isolation performances of the proposed antenna. Fig. 12 shows the simulated and measured realized peak gain and efficiency of the proposed antenna, demonstrating that the experimental results are consistent well with the simulations. The realized peak gain is more than 4.1 dBi over the operating bandwidth, with the maximum of 4.9 dBi achieved at 2.46 GHz. The measured antenna efficiency over 70% and 72% within the operating bandwidth is achieved for TX and RX ports, respectively, with the maximum value of 85% and 86% for two ports at 2.46 GHz, respectively.

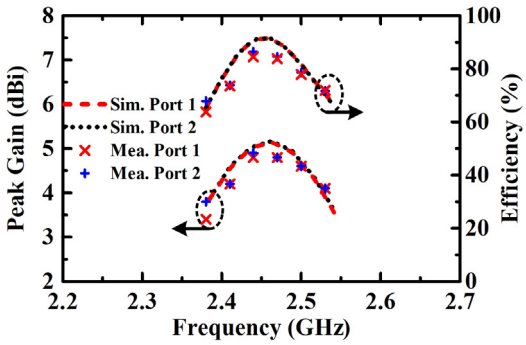

Fig. 12. Simulated and measured gain, and total efficiency of the proposed antenna.

The simulated efficiency is higher than 76% over the operating bandwidth, with the maximum of 92% at 2.46 GHz. Fig. 13 reports the measured and simulated normalized radiation patterns of the proposed antenna at 2.46 GHz. It is seen that the measured results have a good agreement with the simulations, verifying that the proposed antenna has identical radiation properties for the TX and RX ports. In addition, the measured cross polarizations are lower than −30 and −23 dB for E-plane and H-plane in broadside, respectively. It is seen that the cross polarization is relatively high at low elevation angles of H-plane. This phenomenon can be easily explained that the proposed antenna actually behaves as a single PIFA antenna when only one port is excited, owing to the high isolation between the TX and RX antennas. For a regular PIFA antenna, the fringing electric fields along the two nonradiating edges of H-plane cannot cancel out with each other, leading to the high cross polarization at low elevation angles. This is also the inherent radiation property of a regular PIFA antenna. Using patch antennas with a lower profile may be helpful for the relief of this effect. Besides, it is seen that maximum radiation direction for E-plane radiation patterns has a slight squint angle of approximately 30° in Fig. 13. Meanwhile, the gain difference between the broadside angle (theta = 90°) and maximum radiation direction is approximately 1 dB.

To highlight the merits and advantages of the proposed antenna over other reported works on in-band full-duplex antennas, Table II is presented in terms of the antenna type, polarization, method, dimension, impedance bandwidth, port isolation, planar integration, and feeding scheme. As seen, although the antennas in [29] and [31] can achieve higher port isolation with planar integration, both occupy large antenna size and use extra feeding networks for phase mode orthogonality or near-field cancellation. Similarly, the antennas in [27], [28], [44], and [47] not only have large size, high profile, and complex feeding schemes such as quadrifilar IC, BFN, and feeding networks, but also nonplanar and bulky structure. Compared with these works, the proposed antenna achieves co-linear polarization, identical radiation properties, and relatively high isolation for in-band full-duplex systems, with the advantages of compact size, low profile, simple feed, and planar structure, especially suitable for volume-limited and planar in-band full-duplex systems and scenarios.

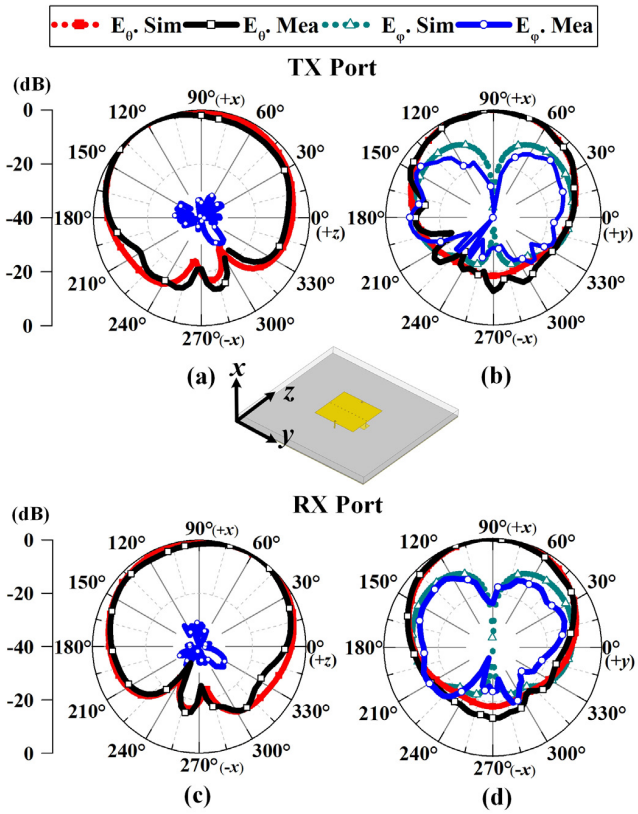

Fig. 13. Simulated and measured normalized radiation patterns of the proposed antenna in *xz* plane and *xy* plane. (a) E-plane and (b) H-plane radiation patterns for TX port (port 1). (c) E-plane and (d) H-plane radiation patterns for RX port (port 2) at 2.46 GHz.

V. Conclusion

In this work, we propose a compact co-linearly polarized microstrip antenna with low profile and identical radiation properties for in-band full-duplex systems. By exploiting an FSR in the central plane of a patch, good isolation is obtained for the TX and RX ports. The FSR contains a metallic vias fence and a strip with a distance away from the ground, serving as a pair of distributed inductor and capacitor. When the FSR resonates, the radiating current is concentrated on the half part of the patch, performing at its half-TM_{10} mode with high port isolation. To verify the proposed antenna, a prototype with the size of $0.25\lambda_0 \times 0.25\lambda_0 \times 0.04\lambda_0$ (λ_0 is the free-space wavelength at center frequency) has been fabricated and tested. The measured results demonstrate a high isolation better than 20 dB and a maximum of 30 dB within the operating bandwidth of 2.40–2.52 GHz. The proposed antenna has the merits of compact size, low profile, simple feed, and planar integration structure, exhibiting potential usage for volume-limited and planar-integrated in-band full-duplex systems and scenarios.

References

[1] A. Sabharwal, P. Schniter, D. Guo, D. W. Bliss, S. Rangarajan, and R. Wichman, "In-band full-duplex wireless: Challenges and opportunities," *IEEE J. Sel. Areas Commun.*, vol. 32, no. 9, pp. 1637–1652, Sep. 2014.

[2] K. E. Kolodziej, B. T. Perry, and J. S. Herd, "In-band full-duplex technology: Techniques and systems survey," *IEEE Trans. Microw. Theory Techn.*, vol. 67, no. 7, pp. 3025–3041, Jul. 2019.

[3] D. Korpi, M. Heino, C. Icheln, K. Haneda, and M. Valkama, "Compact inband full-duplex relays with beyond 100 dB self-interference suppression: Enabling techniques and field measurements," *IEEE Trans. Antennas Propag.*, vol. 65, no. 2, pp. 960–965, Feb. 2017.

[4] Z. Zhang, K. Long, A. V. Vasilakos, and L. Hanzo, "Full-duplex wireless communications: Challenges, solutions, and future research directions," *Proc. IEEE*, vol. 104, no. 7, pp. 1369–1409, Jul. 2016.

[5] Z. Zhang, X. Chai, K. Long, A. V. Vasilakos, and L. Hanzo, "Full duplex techniques for 5G networks: Self-interference cancellation, protocol design, and relay selection," *IEEE Commun. Mag.*, vol. 53, no. 5, pp. 128–137, May 2015.

[6] M. Tsunezawa, K. Takahashi, N. Honma, K. Murata, and K. Nishimori, "Antenna arrangement suitable for full-duplex MIMO," *IEEE Trans. Antennas Propag.*, vol. 65, no. 6, pp. 2966–2974, Jun. 2017.

[7] M. Heino *et al.*, "Recent advances in antenna design and interference cancellation algorithms for in-band full duplex relays," *IEEE Commun. Mag.*, vol. 53, no. 5, pp. 91–101, May 2015.

[8] T. Snow, C. Fulton, and W. J. Chappell, "Transmit–receive duplexing using digital beamforming system to cancel self-interference," *IEEE Trans. Microw. Theory Techn.*, vol. 59, no. 12, pp. 3494–3503, Dec. 2011.

[9] O. N. Alrabadi, A. D. Tatomirescu, M. B. Knudsen, M. Pelosi, and G. F. Pedersen, "Breaking the transmitter–receiver isolation barrier in mobile handsets with spatial duplexing," *IEEE Trans. Antennas Propag.*, vol. 61, no. 4, pp. 2241–2251, Apr. 2013.

[10] P. V. Prasannakumar, M. A. Elmansouri, and D. S. Filipovic, "Wideband decoupling techniques for dual-polarized bi-static simultaneous transmit and receive antenna subsystem," *IEEE Trans. Antennas Propag.*, vol. 65, no. 10, pp. 4991–5001, Oct. 2017.

[11] S. Manshari, S. Koziel, and L. Leifsson, "Compact dual-polarized corrugated horn antenna for satellite communications," *IEEE Trans. Antennas Propag.*, vol. 68, no. 7, pp. 5122–5129, Jul. 2020.

[12] H. Nawaz and I. Tekin, "Dual-polarized, differential fed microstrip patch antennas with very high interport isolation for full-duplex communication," *IEEE Trans. Antennas Propag.*, vol. 65, no. 12, pp. 7355–7360, Dec. 2017.

[13] F. Chen, R. Morawski, and T. Le-Ngoc, "Self-interference channel characterization for wideband 2×2 MIMO full-duplex transceivers using dual-polarized antennas," *IEEE Trans. Antennas Propag.*, vol. 66, no. 4, pp. 1967–1976, Apr. 2018.

[14] H. Nawaz and I. Tekin, "Double-differential-fed, dual-polarized patch antenna with 90 dB interport RF isolation for a 2.4 GHz in-band full-duplex transceiver," *IEEE Antennas Wireless Propag. Lett.*, vol. 17, no. 2, pp. 287–290, Feb. 2018.

[15] H. Nawaz and I. Tekin, "Compact dual-polarized microstrip patch antenna with high interport isolation for 2.5 GHz in-band full-duplex wireless applications," *IET Microw., Antennas Propag.*, vol. 11, no. 7, pp. 976–981, Jun. 2017.

[16] H. Nawaz and I. Tekin, "Dual port single patch antenna with high interport isolation for 2.4 GHz in-band full duplex wireless applications," *Microw. Opt. Technol. Lett.*, vol. 58, no. 7, pp. 1756–1759, Jul. 2016.

[17] Y.-M. Zhang and J.-L. Li, "Differential-series-fed dual-polarized traveling-wave array for full-duplex applications," *IEEE Trans. Antennas Propag.*, vol. 68, no. 5, pp. 4097–4102, May 2020.

[18] Y.-M. Zhang, S. Zhang, J.-L. Li, and G. F. Pedersen, "A dual-polarized linear antenna array with improved isolation using a slotline-based 180° hybrid for full-duplex applications," *IEEE Antennas Wireless Propag. Lett.*, vol. 18, no. 2, pp. 348–352, Feb. 2019.

[19] Y.-M. Zhang and J.-L. Li, "A dual-polarized antenna array with enhanced interport isolation for far-field wireless data and power transfer," *IEEE Trans. Veh. Technol.*, vol. 67, no. 11, pp. 10258–10267, Nov. 2018.

[20] Y. Li, Z. Zhang, J. Zheng, and Z. Feng, "Compact azimuthal omnidirectional dual-polarized antenna using highly isolated colocated slots," *IEEE Trans. Antennas Propag.*, vol. 60, no. 9, pp. 4037–4045, Sep. 2012.

[21] Y. He, Y. Li, W. Sun, Z. Zhang, and P.-Y. Chen, "Dual linearly polarized microstrip antenna using a slot-loaded TM_{50} mode," *IEEE Antennas Wireless Propag. Lett.*, vol. 17, no. 12, pp. 2344–2348, Dec. 2018.

[22] Y. He, Y. Li, W. Sun, and Z. Zhang, "Dual-polarized, high-gain, and low-profile magnetic current array antenna," *IEEE Trans. Antennas Propag.*, vol. 67, no. 2, pp. 1312–1317, Feb. 2019.

[23] Y. He and Y. Li, "Dual-polarized microstrip antennas with capacitive via fence for wide beamwidth and high isolation," *IEEE Trans. Antennas Propag.*, vol. 68, no. 7, pp. 5095–5103, Jul. 2020.

[24] C.-Y.-D. Sim, C.-C. Chang, and J.-S. Row, "Dual-feed dual-polarized patch antenna with low cross polarization and high isolation," *IEEE Trans. Antennas Propag.*, vol. 57, no. 10, pp. 3321–3324, Oct. 2009.

[25] K.-L. Wong and T.-W. Chiou, "Broadband dual-polarized patch antennas fed by capacitively coupled feed and slot-coupled feed," *IEEE Trans. Antennas Propag.*, vol. 50, no. 3, pp. 346–351, Mar. 2002.

[26] E. A. Etellisi, M. A. Elmansouri, and D. S. Filipovic, "In-band full-duplex multimode lens-loaded eight-arm spiral antenna," *IEEE Trans. Antennas Propag.*, vol. 66, no. 4, pp. 2084–2089, Apr. 2018.

[27] R. Lian, T.-Y. Shih, Y. Yin, and N. Behdad, "A high-isolation, ultra-wideband simultaneous transmit and receive antenna with monopole-like radiation characteristics," *IEEE Trans. Antennas Propag.*, vol. 66, no. 2, pp. 1002–1007, Feb. 2018.

[28] D. Wu, Y. Zang, H. Luyen, M. Li, and N. Behdad, "A compact, low-profile simultaneous transmit and receive antenna with monopole-like radiation characteristics," *IEEE Antennas Wireless Propag. Lett.*, vol. 18, no. 4, pp. 611–615, Apr. 2019.

[29] J. Wu, M. Li, and N. Behdad, "A wideband, unidirectional circularly polarized antenna for full-duplex applications," *IEEE Trans. Antennas Propag.*, vol. 66, no. 3, pp. 1559–1563, Mar. 2018.

[30] K. E. Kolodziej, P. T. Hurst, A. J. Fenn, and L. I. Parad, "Ring array antenna with optimized beamformer for simultaneous transmit and receive," in *Proc. IEEE Int. Symp. Antennas Propag.*, Jul. 2012, pp. 1–2.

[31] D. Wu, Y.-X. Sun, B. Wang, and R. Lian, "A compact, monostatic, co-circularly polarized simultaneous transmit and receive (STAR) antenna with high isolation," *IEEE Antennas Wireless Propag. Lett.*, vol. 19, no. 7, pp. 1127–1131, Jul. 2020.

[32] M. Heino, S. N. Venkatasubramanian, C. Icheln, and K. Haneda, "Design of wavetraps for isolation improvement in compact in-band full-duplex relay antennas," *IEEE Trans. Antennas Propag.*, vol. 64, no. 3, pp. 1061–1070, Mar. 2016.

[33] D. Sievenpiper, L. Zhang, R. F. J. Broas, N. G. Alexopolous, and E. Yablonovitch, "High-impedance electromagnetic surfaces with a forbidden frequency band," *IEEE Trans. Microw. Theory Techn.*, vol. 47, no. 11, pp. 2059–2074, Nov. 1999.

[34] F. Yang and Y. Rahmat-Samii, "Microstrip antennas integrated with electromagnetic band-gap (EBG) structures: A low mutual coupling design for array applications," *IEEE Trans. Antennas Propag.*, vol. 51, no. 10, pp. 2936–2946, Oct. 2003.

[35] J.-Y. Lee, S.-H. Kim, and J.-H. Jang, "Reduction of mutual coupling in planar multiple antenna by using 1-D EBG and SRR structures," *IEEE Trans. Antennas Propag.*, vol. 63, no. 9, pp. 4194–4198, Sep. 2015.

[36] X.-J. Lin, Z.-M. Xie, and P.-S. Zhang, "Integrated filtering microstrip duplex antenna array with high isolation," *Int. J. Antennas Propag.*, vol. 2017, pp. 1–8, Jan. 2017.

[37] H. Xu, H. Zhou, S. Gao, H. Wang, and Y. Cheng, "Multimode decoupling technique with independent tuning characteristic for mobile terminals," *IEEE Trans. Antennas Propag.*, vol. 65, no. 12, pp. 6739–6751, Dec. 2017.

[38] K. Iwamoto, M. Heino, K. Haneda, and H. Morikawa, "Design of an antenna decoupling structure for an inband full-duplex collinear dipole array," *IEEE Trans. Antennas Propag.*, vol. 66, no. 7, pp. 3763–3768, Jul. 2018.

[39] A. T. Wegener and W. J. Chappell, "Simultaneous transmit and receive with a small planar array," in *IEEE MTT-S Int. Microw. Symp. Dig.*, Montreal, QC, Canada, Jun. 2012, pp. 1–3.

[40] A. T. Wegener and W. J. Chappell, "High isolation in antenna arrays for simultaneous transmit and receive," in *Proc. IEEE Int. Symp. Phased Array Syst. Technol.*, Oct. 2013, pp. 593–597.

[41] J. Ha, M. A. Elmansouri, P. V. Prasannakumar, and D. S. Filipovic, "Monostatic co-polarized full-duplex antenna with left-or right-hand circular polarization," *IEEE Trans. Antennas Propag.*, vol. 65, no. 10, pp. 5103–5111, Oct. 2017.

[42] Z. Zhou, Y. Li, J. Hu, Y. He, Z. Zhang, and P.-Y. Chen, "Monostatic copolarized simultaneous transmit and receive (STAR) antenna by integrated single-layer design," *IEEE Antennas Wireless Propag. Lett.*, vol. 18, no. 3, pp. 472–476, Mar. 2019.

[43] P. V. Prasannakumar, M. A. Elmansouri, and D. S. Filipovic, "Broadband reflector antenna with high isolation feed for full-duplex applications," *IEEE Trans. Antennas Propag.*, vol. 66, no. 5, pp. 2281–2290, May 2018.

[44] A. H. Abdelrahman and D. S. Filipovic, "Antenna system for full-duplex operation of handheld radios," *IEEE Trans. Antennas Propag.*, vol. 67, no. 1, pp. 522–530, Jan. 2019.

[45] L. Sun, Y. Li, Z. Zhang, and Z. Feng, "Compact co-horizontally polarized full-duplex antenna with omnidirectional patterns," *IEEE Antennas Wireless Propag. Lett.*, vol. 18, no. 6, pp. 1154–1158, Jun. 2019.
[46] E. A. Etellisi, M. A. Elmansouri, and D. Filipovic, "Broadband full-duplex monostatic circular-antenna arrays: Circular arrays reaching simultaneous transmit and receive operation," *IEEE Antennas Propag. Mag.*, vol. 60, no. 5, pp. 62–77, Oct. 2018.
[47] M. R. Nikkhah, J. Wu, H. Luyen, and N. Behdad, "A concurrently dual-polarized, simultaneous transmit and receive (STAR) antenna," *IEEE Trans. Antennas Propag.*, vol. 68, no. 8, pp. 5935–5944, Aug. 2020.
[48] E. A. Etellisi, M. A. Elmansouri, and D. S. Filipovic, "Wideband monostatic simultaneous transmit and receive (STAR) antenna," *IEEE Trans. Antennas Propag.*, vol. 64, no. 1, pp. 6–15, Jan. 2016.
[49] E. A. Etellisi, M. A. Elmansouri, and D. S. Filipovic, "Wideband multimode monostatic spiral antenna STAR subsystem," *IEEE Trans. Antennas Propag.*, vol. 65, no. 4, pp. 1845–1854, Apr. 2017.
[50] M. A. Elmansouri, A. J. Kee, and D. S. Filipovic, "Wideband antenna array for simultaneous transmit and receive (STAR) applications," *IEEE Antennas Wireless Propag. Lett.*, vol. 16, pp. 1277–1280, 2017.
[51] Y.-M. Zhang and J.-L. Li, "Analyses and full-duplex applications of circularly polarized OAM arrays using sequentially rotated configuration," *IEEE Trans. Antennas Propag.*, vol. 66, no. 12, pp. 7010–7020, Dec. 2018.
[52] C. A. Balanis, *Antenna Theory: Analysis and Design*, 4th ed. Hoboken, NJ, USA: Wiley, 2016.

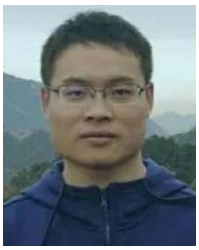

Yijing He (Graduate Student Member, IEEE) received the B.S. degree in electronic and information engineering from Xidian University, Xi'an, China, in 2016. He is currently pursuing the Ph.D. degree in electronic engineering with Tsinghua University, Beijing, China.

His current research interests include microstrip antennas, MIMO and diversity antennas, metamaterials, plasmonics, metasurface, and metamaterial-related antennas.

Mr. He was a recipient of the Graduate Academic Newcomer Award from the first National Metamaterials Conference in 2019. He serves as a Reviewer for nearly ten international academic journals including the IEEE TRANSACTIONS ON ANTENNAS AND PROPAGATION, IEEE ANTENNAS AND WIRELESS PROPAGATION LETTERS, IEEE SENSORS JOURNAL, IEEE JOURNAL OF ELECTROMAGNETICS, RF AND MICROWAVES IN MEDICINE AND BIOLOGY, IEEE ACCESS, *IET Microwaves, Antennas & Propagation*, *Microwave and Optical Technology Letters*, and *International Journal of RF and Microwave Computer-Aided Engineering*.

Yue Li (Senior Member, IEEE) received the B.S. degree in telecommunication engineering from Zhejiang University, Hangzhou, China, in 2007, and the Ph.D. degree in electronic engineering from Tsinghua University, Beijing, China, in 2012.

In June 2012, he joined the Department of Electronic Engineering, Tsinghua University, as a Post-Doctoral Fellow. In December 2013, he joined the Department of Electrical and Systems Engineering, University of Pennsylvania, Philadelphia, PA, USA, as a Research Scholar. He was a Visiting Scholar with the Institute for Infocomm Research (I2R), A*STAR, Singapore, in 2010, and the Hawaii Center of Advanced Communication (HCAC), University of Hawai?i at Mānoa, Honolulu, HI, USA, in 2012. Since January 2016, he has been with Tsinghua University, where he is currently an Assistant Professor and an Associate Professor with the Department of Electronic Engineering. He has authored or coauthored over 150 journal articles and 45 international conference articles, and holds 20 granted Chinese patents. His current research interests include metamaterials, plasmonics, electromagnetics, nanocircuits, mobile and handset antennas, MIMO and diversity antennas, and millimeter-wave antennas and arrays.

Dr. Li was a recipient of the Issac Koga Gold Medal from URSI General Assembly in 2017; the Second Prize of Science and Technology Award of China Institute of Communications in 2017; the Young Scientist Awards from the conferences of PIERS 2019, ACES 2018, AT-RASC 2018, AP-RASC 2016, EMTS 2016, and URSI GASS 2014; the best paper awards from the conferences of APCAP 2020/2017, UCMMT 2020, ISAP 2019, CSQRWC 2018, NCMMW 2018/2017, NCANT 2019/2017, ISAPE 2016, and ICMMT 2020/2016; the Outstanding Doctoral Dissertation of Beijing Municipality in 2013, and the Principal Scholarship of Tsinghua University in 2011. He is serving as an Associate Editor for IEEE TRANSACTIONS ON ANTENNAS AND PROPAGATION, IEEE ANTENNAS AND WIRELESS PROPAGATION LETTERS, *Microwave and Optical Technology Letters*, and *Computer Applications in Engineering Education*, and the Editorial Board of Scientific Report.